Journal of Chemical Technology and Metallurgy, 53, 2, 2018, 311-323

COMPARATIVE ANALYSIS OF ELECTROCHEMICAL CORROSION BEHAVIOR AND INHIBITION OF 2101 DUPLEX AND 301 AUSTENITIC STAINLESS STEEL IN 4-CYANOBENZENE/6M H_2SO_4 SOLUTION

Roland Tolulope Loto

Department of Mechanical Engineering, Covenant University
Ota, Ogun State, Nigeria
E-mail: tolu.loto@gmail.com

Received 11 August 2017
Accepted 15 December 2017

ABSTRACT

Corrosion inhibition effect of 4-cyanobenzene on 2101 duplex (2101SS) and 301 austenitic (301SS) stainless steels was studied by potentiodynamic polarization, corrosion potential measurement, optical microscopy and FTIR spectroscopy. The results showed the compound to be effective with inhibition efficiency of 98.75 % and 99.54 % for both steels. Corrosion potential of 2101SS and 301SS decreased from -0.067$V_{Ag/AgCl}$ to -0.182$V_{Ag/AgCl}$, and -0.145$V_{Ag/AgCl}$ to -0.196$V_{Ag/AgCl}$. Identified functional groups partially adsorbed onto both steels. The thermodynamic calculations showed physicochemical interaction according to Langmuir and Freundlich isotherms. The optical images showed a worn out morphology for 2101SS and an etched for 301SS. The compound studied is an anodic type inhibitor on both steels.

Keywords: corrosion, steel, acid, inhibitor, adsorption.

INTRODUCTION

Stainless steels are generally used in industrial environments where economic cost are a critical issue, as they offer improved corrosion resistance in relation to carbon steels [1, 2]. They are increasingly applied in oil and gas applications, automotive, propulsion shaft for high speed craft and food processing products, as well as medical and health equipment due to their good corrosion resistance and mechanical properties. The corrosion resistance of stainless steels is related to the formation and breakdown of passive film on the metal surface in the solutions with aggressive anions resulting in localized corrosion such as pitting. This localized dissolution of metallic alloys in specific aggressive environments is one of the most common and catastrophic causes of failure of metallic structures. The pitting process has been described as random, sporadic and stochastic and the prediction of the time and location of events remains extremely difficult. Anodic dissolution proceeds while the major part of metal surface remains passive.

The ability of stainless steel to repassivate after breakdown of its passive film in corrosive solutions is the major factor in determining its resistance to localized failures. One of the most effective methods of improving the corrosion resistance of metallic alloys is through the use of organic chemical compounds for corrosion inhibition. Corrosion inhibitors are extensively used for acid pickling, industrial acid cleaning, acid descaling and oil well acidizing. The performance of organic compounds is strongly dependent on the structure and chemical properties of the protective film formed on the metal surface, which is majorly ascribed to the effects of the functional groups within their molecular structure [3]. Compounds containing heteroatoms have been found to serve as good inhibitors of corrosion and their inhibiting action has been explained in terms of the number of free electron pairs, the p-orbital character of free electrons and the electron density around the heteroatoms [4 - 6]. Inhibition mechanisms are thought to involve competitive adsorption or formation of more protective passive film [7]. Although there are several studies on the corrosion inhibition effects of organic compounds in acidic solutions, there are only a few concerning steel corrosion

in aqueous solutions [8 - 10]. The use of chemical inhibitors to decrease the rate of corrosion processes is quite varied. In the oil extraction and processing industries, inhibitors have always been considered to be the first line of control against corrosion. In view of this, the corrosion inhibition effect of 4-cyanobenzene on 2101 duplex and 301 austenitic stainless steel in high molar concentration of sulphuric acid was investigated through potentiodynamic polarization, optical microscopy analysis, FTIR spectroscopy and open circuit potential measurement.

EXPERIMENTAL

Materials and preparation

2101 duplex stainless steel (2101SS) and 301 austenitic stainless steel (301SS) obtained commercially have nominal compositions as shown in Table 1. The steel specimens after machining were smoothened with silicon carbide papers (80, 320, 600, 800 and 1000 grit) before being washed with distilled water and acetone, and kept in a desiccator for corrosion potential measurement and potentiodynamic polarization tests according to ASTM G1 - 03(2011) [11]. 4-cyanobenzene obtained from BOC Sciences, USA, is the organic compound evaluated for its corrosion inhibiting properties. It is a colourless, slightly viscous aromatic heterocyclic compound with a molar mass of 103.12 g/mol and a molecular formula of C_7H_5N. The compound was prepared in molar concentrations of 2.42 x 10^2, 4.85 x 10^2, 7.27 x 10^2, 9.70 x 10^2 and 1.2 x 10^1 in 200 mL of 6M H_2SO_4 solution, prepared from analar grade of H_2SO_4 acid (98 %) with distilled water.

Potentiodynamic polarization technique

Polarization measurements were carried out at 30°C using a three electrode system and glass cell containing 200 mL of the corrosive test solution with Digi-Ivy 2311 electrochemical workstation. 2101SS and 301SS electrodes mounted in acrylic resin with an exposed surface area of 2.54 cm^2 and 0.72 cm^2 were prepared according to ASTM G59-97(2014) [12]. The polarization plots were obtained at a scan rate of 0.0015 V/s between potentials of −1V and +2V according to ASTM G102-89(2015) [13]. A platinum rod was used as the counter electrode and a silver chloride electrode (Ag/AgCl) as the reference electrode. Corrosion current density (j_{cr}) and corrosion potential (E_{cr}) values were obtained using the Tafel extrapolation method. The corrosion rate (r) and the inhibition efficiency (η_2, %) were calculated from the mathematical relationship:

$$C_R = \frac{0.00327 \times J_{corr} \times E_{qv}}{D} \quad (1)$$

where j_{corr} is the current density in A/cm^2, D is the density in g/cm^3; E_{qv} is the sample equivalent weight in grams, 0.00327 is a constant for corrosion rate calculation in mm/y [14].

Open circuit potential measurement

OCP measurements were obtained at a step potential of 0.05 V/s with two-electrode electrochemical cell consisting of Ag/AgCl reference electrode and resin mounted steel specimens (exposed surface of 2.54 cm^2) as the working electrode, connected to Digi-Ivy 2311 potentiostat according to ASTM G69 – 12(2012) [15]. The electrodes were fully immersed in 200 ml of the test media at specific concentrations of 4CB for 2700 s.

Infrared spectroscopy and optical microscopy characterization

4CB/6M H_2SO_4 solution (before and after the corrosion test) was exposed to specific range of infrared ray beams from Bruker Alpha FTIR spectrometer at wavelength range of 375 to 7500 cm^{-1} and resolution of 0.9 cm^{-1}. The transmittance and reflectance of the infrared beams at various frequencies were decoded and transformed into an FTIR absorption plot consisting of spectra peaks. The spectral pattern was evaluated and equated with IR absorption table to identify the functional groups responsible for corrosion inhibition. Optical images of the corroded and inhibited 2101SS and

Table 1. Percentage Nominal Composition of 2101SS and 301SS.

Element Symbol	Mo	Si	Ni	Cr	Mn	P	N	C	Fe
% Composition (2101SS)	0.4	1	1.8	22.8	4	0.04	0.2	0.03	69.7
% Composition (301SS)	0.0	1	8.0	16.0	2	0.045	0.1	0.15	72.7

301SS surface morphologies from optical microscopy were analysed after the electrochemical test with Omax trinocular with the aid of ToupCam analytical software.

RESULTS AND DISCUSSION

Polarization studies

The potentiodynamic polarization curves of 2101SS and 301SS (Figs. 1 and 2) showed similar anodic/cathodic polarization behavior for localized corrosion of stainless steel [16], consisting of active dissolution, passivity, and a rapid increase in the current density due to pitting. The effect of 4CB is clearly shown from the contrast in polarization behavior of both steels, at 0 % 4CB and 0.25 % - 1.5 % 4CB concentrations. At 0 % 4CB the current density of 2101SS and 301SS are 1.35 x 10^3 A/cm^2 and 4.17 x 10^3 A/cm^2, addition of 4CB at 0.25 % significantly lowers their current density to 5.33 x 10^5 and 3.78 x 10^5, respectively. The corrosion potentials of both steels also experienced a large anodic shift upon addition of 4CB compound at 0.25 % 4CB. The shift to anodic values is due to similar electrochemical action of 4CB molecules in counteracting the action of SO_4^{2-} ions in the acid solution. The corrosion potential of 301SS tends to be more electronegative, probably due to its austenite microstructure stabilized by its higher nickel content than 2101SS, but lower chromium content. As a result the alloy surface of 301SS tends to more easily form soft acid, from the concept Lewis acid-base theory resulting in greater adsorption of 4CB molecules due to higher preadsorption of SO_4^{2-} ions [17].

This assumption is confirmed from the relatively higher corrosion rate of 301SS than 2101SS at 0 % 4CB (Tables 2 and 3), however its higher adsorption of 4CB protonated molecules results in higher inhibition efficiency. The anodic shift in corrosion potential shows that surface coverage of the reacting sites on the steels surface predominantly hinders the oxidation reaction of the corrosion mechanism. This is due to release of fewer electrons which slows down the anodic reaction mechanism. Changes in anodic Tafel slope values in comparison to cathodic Tafel slope for 301SS and 2101SS is as a result of the electrochemical action of 4CB on the formation of surface oxides from the slow electron transfer step which eventually changes due to changes in the electrode substrate, rate controlling step and influence of potential controlled conditions [18, 19]. 4CB forms soluble, complex cationic molecules with valence metal anions of both steels, inactivating them in the acid solution so they cannot normally react with the corrosive ions to produce surface precipitates. Though 2101SS and 301SS have different corrosion

Table 2. Potentiodynamic polarization results for 2101SS in 6M H_2SO_4 (0 % - 1.25 % 4CB).

Sample	4CB conc. (%)	4CB conc. (M)	Corrosion Rate (mm/y)	4CB Inhibition Efficiency (%)	Corrosion Current (A)	Corrosion Current Density (A/cm^2)	Corrosion Potential (V)	Polarization Resistance, R_p (Ω)	Cathodic Tafel Slope, B_c (V/dec)	Anodic Tafel Slope, B_a (V/dec)
A	0	0	14.22	0	3.44E-03	1.35E-03	0.006	1538.21	-0.677	2.567
B	0.25	2.42E-02	0.56	96.06	1.35E-04	5.33E-05	0.098	189.80	-8.080	5.503
C	0.5	4.85E-02	0.19	98.66	4.61E-05	1.81E-05	0.162	557.50	-8.550	1.753
D	0.75	7.27E-02	0.18	98.75	4.30E-05	1.69E-05	0.081	597.60	-8.579	6.807
E	1	9.70E-02	0.19	98.63	4.71E-05	1.85E-05	0.106	545.70	-7.112	9.841
F	1.25	1.21E-01	0.24	98.28	5.91E-05	2.33E-05	0.110	436.40	-7.051	10.070

Table 3. Potentiodynamic polarization results for 301SS in 6M H_2SO_4 (0 % - 1.25 % 4CB).

Sample	4CB conc. (%)	4CB conc. (M)	Corrosion Rate (mm/y)	4CB Inhibition Efficiency (%)	Corrosion Current (A)	Corrosion Current Density (A/cm^2)	Corrosion Potential (V)	Polarization Resistance, R_p (Ω)	Cathodic Tafel Slope, B_c (V/dec)	Anodic Tafel Slope, B_a (V/dec)
A	0	0	32.05	0	3.00E-03	4.17E-03	-0.364	43920.00	-0.602	2.971
B	0.25	2.42E-02	0.29	99.09	2.72E-05	3.78E-05	-0.269	1846.00	-8.494	4.948
C	0.5	4.85E-02	0.15	99.54	1.39E-05	1.93E-05	-0.249	945.30	-7.387	7.847
D	0.75	7.27E-02	0.33	98.96	3.12E-05	4.33E-05	-0.229	823.50	-7.587	14.860
E	1	9.70E-02	0.16	99.50	1.50E-05	2.08E-05	-0.209	1718.00	-8.785	4.657
F	1.25	1.21E-01	0.18	99.45	1.65E-05	2.29E-05	-0.270	1557.00	-8.321	9.918

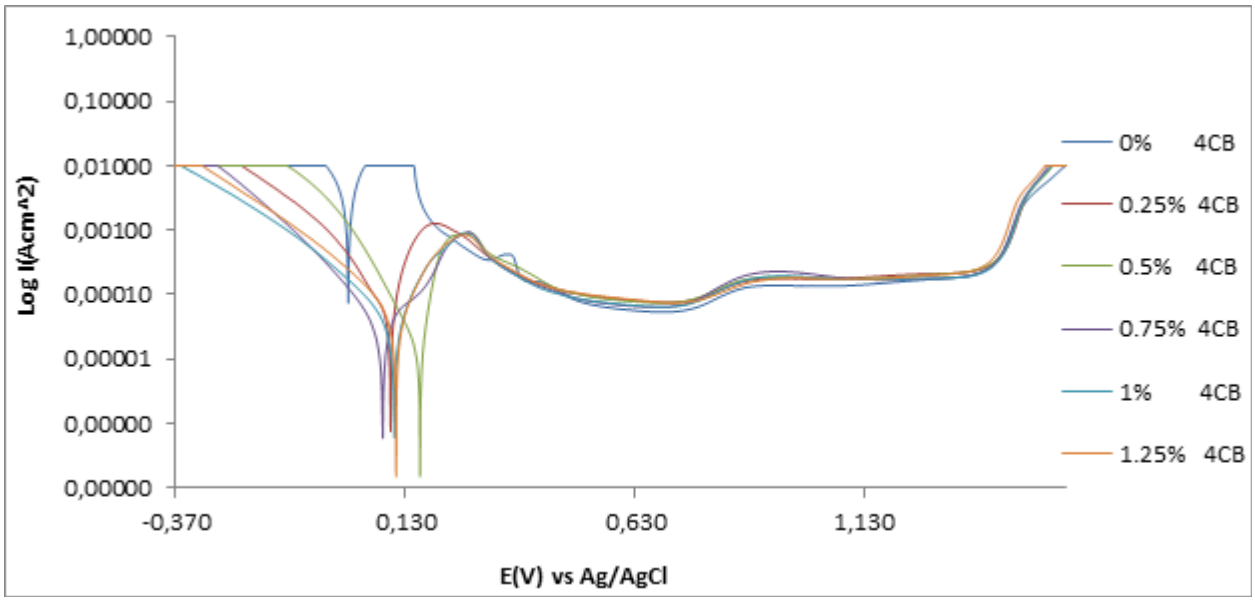

Fig. 1. Potentiodynamic polarization curves for 2101SS in 6M H_2SO_4 (0 % - 1.5 % 4CB).

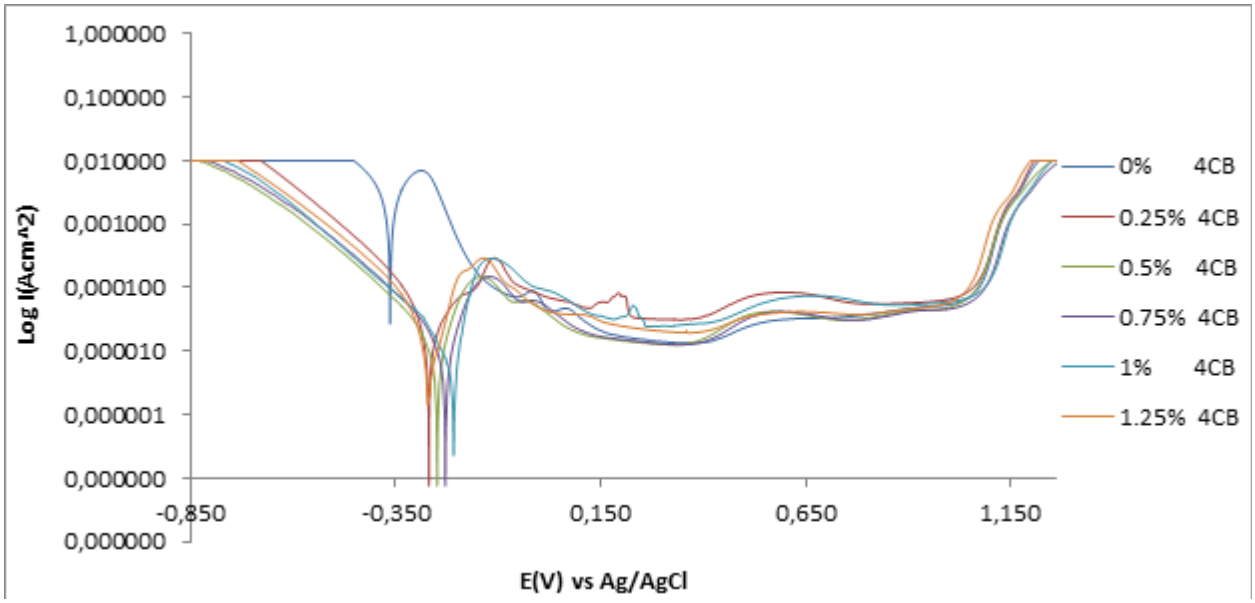

Fig. 2. Potentiodynamic polarization curves for 301SS in 6M H_2SO_4 (0 % - 1.5 % 4CB).

rates in the absence of 4CB compound, the inhibition efficiencies of 4CB on both steels are generally the same despite different metallurgical structure and composition because 4CB establishes a controlled equilibrium of anion and cation diffusion across it across the metal inhibitor interface. The maximum change in corrosion potential of 2101SS in H_2SO_4 solution is 156 mV, while for 301SS the change in corrosion potential is 155 mV, thus 4CB is an anodic type inhibitor in H_2SO_4 solution for both steels [20].

Pitting corrosion and passivation characteristics

Potentiostatic parameters of 2101SS and 301SS are shown in Table 4. The molecular interaction of 4CB on the 2101SS surface marginally increased the pitting corrosion resistance of the steel from 1.313$V_{Ag/AgCl}$ (0 % 4CB) to 1.348$V_{Ag/AgCl}$ (0.25 % 4CB) with a corresponding change in pitting corrosion current. Increase in 4CB concentration had no further effect of the pitting potential of 2101SS beyond 0.25 % 4CB. The effect of 4CB on 301SS is less proportional as its pitting potential

Table 4. Potentiostatic data of pitting and passivation potentials for 2101SS and 301SS in 6M H_2SO_4/ (0 % - 1.5 % 4CB) solution.

2101SS						
Sample	4CB Concentration (M)	Pitting Potential (V), E_{pitt}	Current at E_{pitt} (A)	Passivation Potential (V)	Current at Passivation Potential (A)	Passivation Range (V)
A	0	1.313	1.80E-04	0.078	9.94E-03	1.235
B	2.42E-02	1.348	2.20E-04	0.149	6.70E-04	1.199
C	4.85E-02	1.348	2.20E-04	0.209	4.90E-04	1.139
D	7.27E-02	1.348	1.90E-04	0.215	4.70E-04	1.133
E	9.70E-02	1.348	1.90E-04	0.209	4.70E-04	1.139
F	1.21E-01	1.348	2.20E-04	0.203	4.80E-04	1.145
301SS						
Sample	4CB Concentration (M)	Pitting Potential (V), E_{pitt}	Current at E_{pitt} (A)	Passivation Potential (V)	Current at Passivation Potential (A)	Passivation Range (V)
A	0	1.009	0.0E+00	-0.323	5.00E-03	1.332
B	2.42E-02	1.006	6.73E-05	-0.131	1.87E-04	1.137
C	4.85E-02	1.017	5.37E-05	-0.182	9.54E-05	1.199
D	7.27E-02	1.014	4.81E-05	-0.166	8.63E-05	1.180
E	9.70E-02	1.044	6.87E-05	-0.155	1.67E-04	1.199
F	1.21E-01	1.003	5.75E-05	-0.168	2.06E-04	1.171

varied with 4CB concentration. At 0.25 % 4CB and 1.5 % 4CB, the pitting potential decreased probably due to the interference of 4CB on the passivation behavior of the steel at high applied potentials. Beyond the pitting potential region of the plot transpassive dissolution occurs before stable pitting due to oxidative dissolution of Cr oxide [21]. Cr(III) is oxidized to Cr(VI) and the protective Cr(III) in the passive film is removed in stainless steels polarized above the transpassive potential [22 - 24]. 301SS showed a stronger tendency to passivate following anodic polarization in comparison to 2101SS at 0 % 4CB from observation of the polarization plots; however this advantage is negligible as 2101 exhibited lower corrosion rates and higher pitting potential in the presence of 4CB compound.

Observation of the passivation potentials of both steels shows that 4CB interferes with their passivation behavior, as a result accelerating the formation of a passive protective film. The passivation potential for 2101SS at 0% 4CB is $0.078V_{Ag/AgCl}$, while the corresponding value for 301SS is $-0.323V_{Ag/AgCl}$. At 0.25% 4CB the passivation potential of both steels has shifted to $0.149V_{Ag/AgCl}$ and $-0.131V_{Ag/AgCl}$ respectively, due to significant decrease in metastable pitting activity of both steels. During metastable pitting process, the passive film on surface is locally damaged first, then the metal dissolution occurs before the surface repassivates. In the absence of 4CB (0% 4CB) metastable pitting event is visible in contrast to 4CB addition (0.25%-1.5%). The effect of 4CB on the pitting corrosion resistance of 2101 and 301SS under applied potential may be relatively marginal, its effect of the passivation behavior and hence the localized corrosion resistance of the steel is significant. The decrease in passivation range of both steels after 0% 4CB is due to the absence of metastable pitting events as 4CB enhances the repassivation capacity of both steels.

Open circuit potential measurement

Fig. 3 shows the variation of corrosion potential with time for 2101SS and 301SS in uninhibited and inhibited 6M H_2SO_4 solution at 37°C during 2700 s of immersion. The variation in corrosion potential for the inhibited stainless steel specimens significantly contrasts the uninhibited steels. The anodic inhibiting nature of 4CB induces a shift in corrosion potential of inhibited 2101SS and 301SS to less noble values due to the adsorption of 4CB onto the steel surfaces resulting in effective surface coverage. Potentiodynamic studies shows that the inhibition efficiency of 4CB on the stainless steels is above 90 % however efficiency values for 301SS tends to be marginally higher. This observation aligns with the

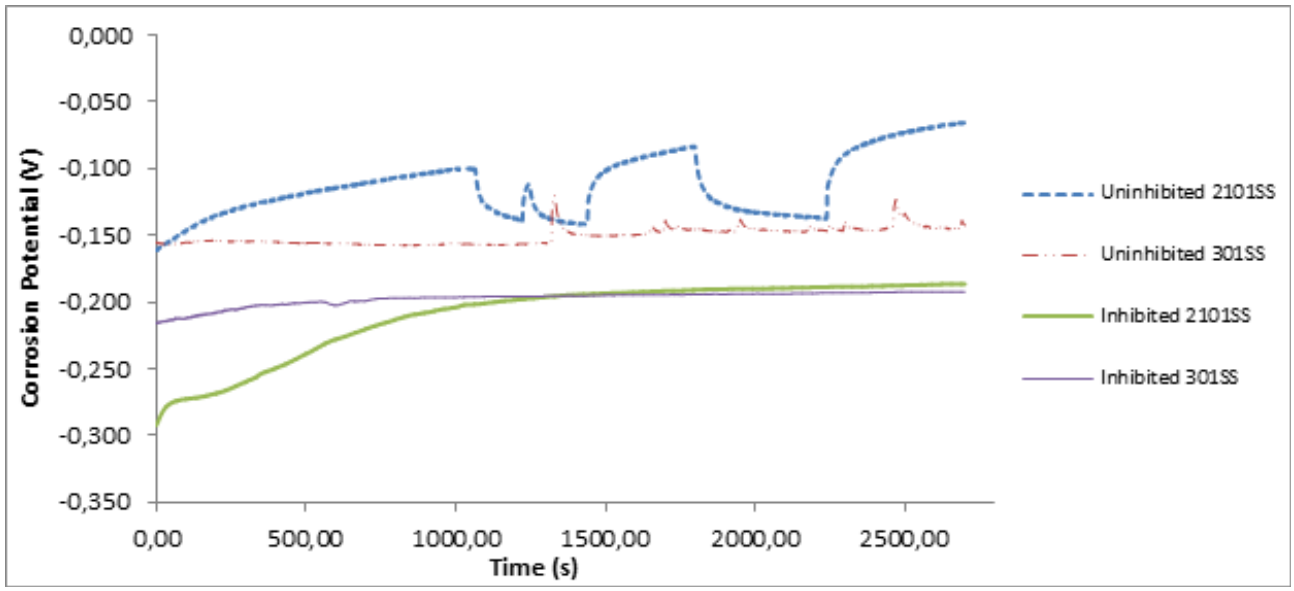

Fig. 3. Variation of corrosion potential with time for 2101SS and 301SS specimen immersed in test solution at 37°C.

observation in Fig. 3 for the inhibited steels in the first 1160 s of exposure. 4CB adsorption on 301SS shifted the corrosion potential from -0.216$V_{Ag/AgCl}$ to a generally constant value of -0.197$V_{Ag/AgCl}$ at 740 s due to passivation and film formation of 4CB adsorption on the steel. The change in corrosion potential for 301SS is small compared to 2101SS due to the tendency of 301SS to form Lewis base as earlier mentioned from preadsorbed corrosive species, resulting in strong adsorption of 4CB molecules. Studying the corrosion potential variation of inhibited 2101SS a large potential shift can be observed from -0.292$V_{Ag/AgCl}$ to -0.196$V_{Ag/AgCl}$ at 1160 s beyond which the corrosion potentials of both steels are generally stable. 4CB tends to adsorb much strongly on 301SS than 2101SS from observation of the corrosion potential before 1160 s. In the first 20 s of exposure, the corrosion potential of 2101SS rose sharply to -0.280$V_{Ag/AgCl}$ after which there is a delay till 145 s at -0.270$V_{Ag/AgCl}$. This is probably due to competitive adsorption between protonated 4CB molecules and oxygen atoms onto the steel resulting in passivation and or breakage in the passive film established by the 4CB due to controlled diffusion of corrosive anions.

The pitting mechanisms of stainless steels are always related to the breakdown and repassivation of the passive film. The variation in corrosion potential for the uninhibited steel specimens shows active passive behaviour due to pit initiation and passivation of both steels. The corrosion potential of 301SS remained generally constant throughout the exposure period with intermittent potential transients between 1281.66$V_{Ag/AgCl}$ and 1367.01$V_{Ag/AgCl}$, 1596.86$V_{Ag/AgCl}$ and 1734.81$V_{Ag/AgCl}$, 1898.86$V_{Ag/AgCl}$ and 1971.22$V_{Ag/AgCl}$, etc. These transients are due to initiation of metastable pits within the oxide surface film, on sites such as surface flaws, inclusions, impurities, etc. [25]. The corrosion potential of the uninhibited 2101SS remained active, consistently increasing from the onset of the exposure period. Passivation behavior was observed at -0.100$V_{Ag/AgCl}$ and -0.085$V_{Ag/AgCl}$ which significantly interrupted the increase in corrosion potential of the steel. This behavior is due to the dissolution and brief repassivation of the passive film of the steel.

FTIR spectroscopy analysis

The functional groups in 4CB compound responsible for adsorption and corrosion inhibition of 2101SS and 301SS were identified on Table 5 and matched with the FTIR Table [26, 27]. Fig. 4 shows the spectra plots of the test solution before corrosion, and after corrosion with 2101SS and 301SS. Observation of Table 5 shows the general decrease in strength of peak intensities of 4CB for 2101SS and 301SS due to partial adsorption of the functional groups onto the steel's surfaces, however the peak intensities for 301SS decrease further than the values obtained for 2101SS due to greater adsorption of identified 4CB functional groups. Earlier discussion has shown that 301SS, due to its tendency to easily form

Table 5. Frequencies and adsorption peaks of FTIR spectroscopy of 6M H_2SO_4/4CB compound before and after 2101SS and 301SS corrosion.

Calculated Wavenumber (cm^{-1})	Control Peak Intensity (%)	2101SS Peak Intensity (%)	301SS Peak Intensity (%)	Theoretical wavenumber (cm^{-1})	Bond	Functional group
				900–675	C–H "oop"	aromatics
				910–665	N–H wag	primary, secondary amines
899.49	0.4373	0.4214	0.3941	1000–650	=C–H bend	alkenes
				1250–1020	C–N stretch	aliphatic amines
1046.34	0.3197	0.3187	0.2980	1320–1000	C–O stretch	alcohols, carboxylic acids, esters, ethers
1170.76	0.3676	0.3500	0.3338	1300–1150	C–H wag ($–CH_2X$)	alkyl halides
				1335–1250	C–N stretch	aromatic amines
1297.22	0.6829	0.6399	0.6256	1360–1290	N–O symmetric stretch	nitro compounds
1582.77	0.6666	0.6439	0.6326	1650–1580	N–H bend	primary amines
1654.16	0.5912	0.5723	0.5608	1680–1640	–C=C– stretch	alkenes

Lewis base compared 2101, thus higher corrosion rate values would naturally experience more adsorption of 4CB molecules onto its surface as a result of inability of its passive film to sufficiently protect it in the presence of corrosive anions. Slightly higher adsorption was observed for aromatics, aromatic amines, nitro compounds, and primary and secondary amines functional groups consisting of the C–H oop, C–N stretch bonds, N–H wag, N–O symmetric stretch. This observation indicates the formation of multi-molecular layer of adsorption between 4CB compound and stainless steels. This also supports the mechanism of physiochemical adsorption.

Molecular adsorption is influenced by the surface charge of the steels and the chemical structure of the inhibiting compound. SO_4^{2-} ions in the inhibited solution adsorbed onto the steel's surfaces through creation of oriented dipoles and consequently enabling electrolytic diffusion of protonated molecules of 4CB.

Adsorption Isotherm

The mechanism of 4CB adsorption on 2101SS and 301SS surface can be further elaborated through adsorption isotherms. The adsorption mechanisms are the product of electrostatic attraction and covalent bond-

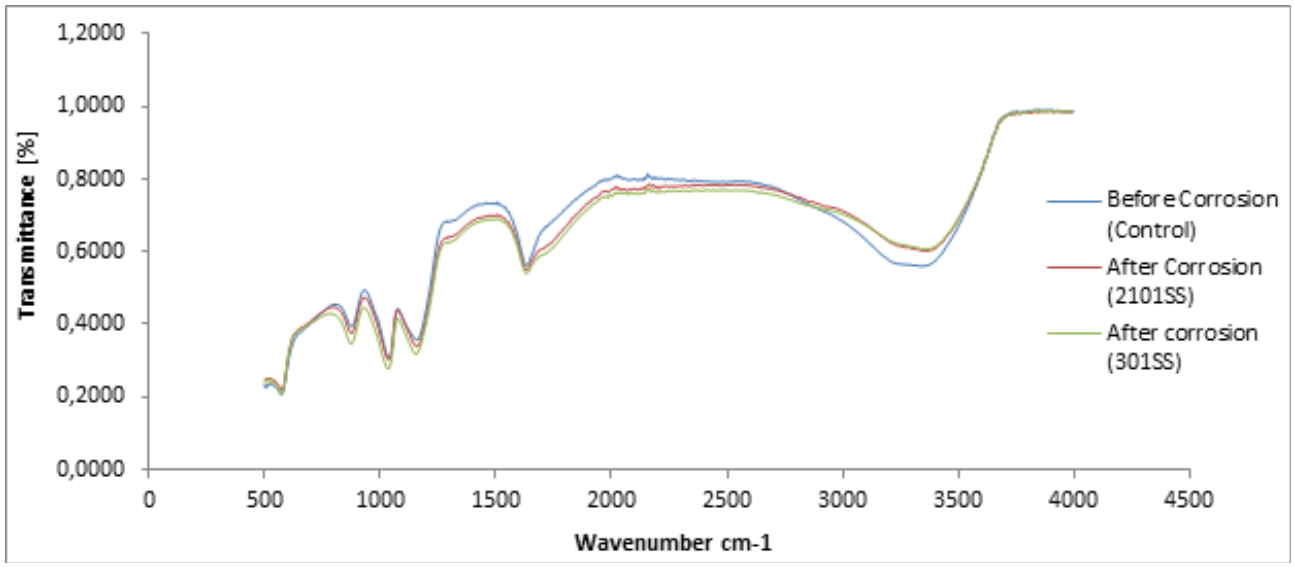

Fig. 4. FTIR spectra of 4CB compound in 6M H_2SO_4 solution before and after 2101SS and 301SS corrosion.

ing between the stainless steel surfaces and the valence electrons within the hetero-atoms of 4CB, involving the removal of 4CB from the acid solution on contact with the adsorbent [28, 29]. These mechanisms are relatively complex and depend on the property of the interface between the steel and acid solution, amount and nature of surface oxide groups and functional groups of the inhibiting compound. Langmuir and Freundlich isotherm models produced the best fit as shown from Figs. 5 - 8 according to the following equations.

$$\theta = \left[\frac{K_{ads} C_{4CB}}{1+K_{ads} C_{4CB}}\right] \quad (2)$$

where θ is the extent of 4CB adsorbed per unit weight on 2101SS and 301SS surfaces at equilibrium, C_{4CB} is 4CB concentration and K_{ads} is the equilibrium constant of the adsorption mechanism. Adsorption plots of $\frac{C_{4CB}}{\theta}$ vs C_{4CB} strongly aligns with Langmuir adsorption isotherm (Fig. 5 and 6), having a correlation coefficient of 1 for 2101SS and 0.9999 for 301SS. Langmuir isotherm assumes monolayer layer adsorption which occurs at specific reaction sites on the steel surfaces. The adsorptions are identical, equivalent and no lateral interaction between the adsorbed molecules exists [30].

$$\theta = KC^n \quad (3)$$

$$\log \theta = n \log C + \log K_{ads} \quad (4)$$

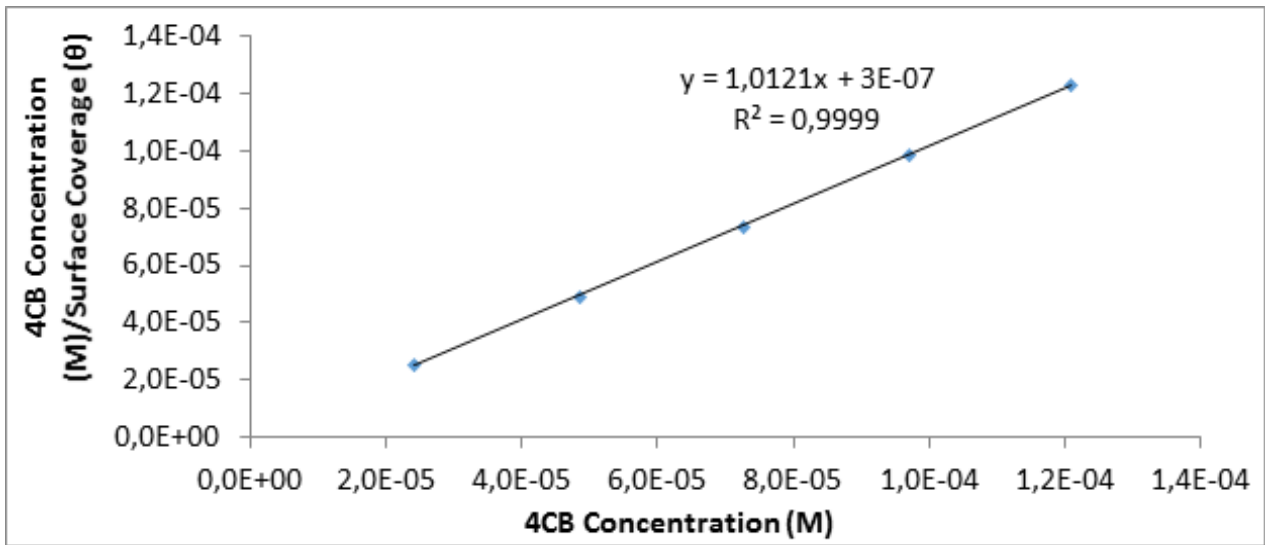

Fig. 5. Plot of $\frac{C}{\theta}$ versus 4CB concentration in 6M H_2SO_4 for 2101SS.

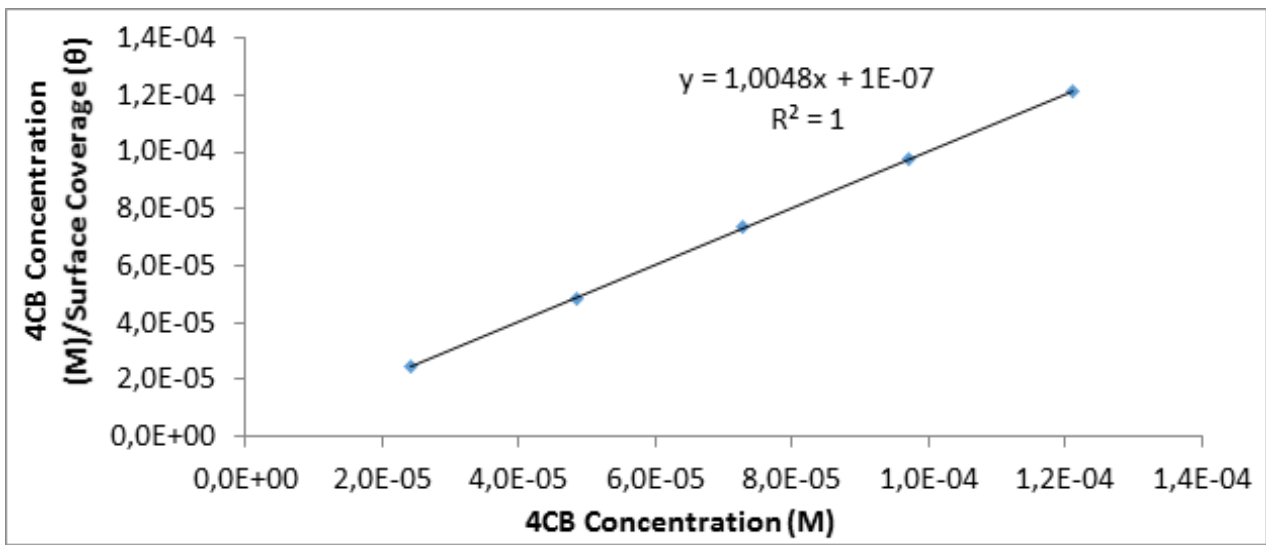

Fig. 6. Plot of $\frac{C}{\theta}$ versus 4CB concentration in 6M H_2SO_4 for 301SS.

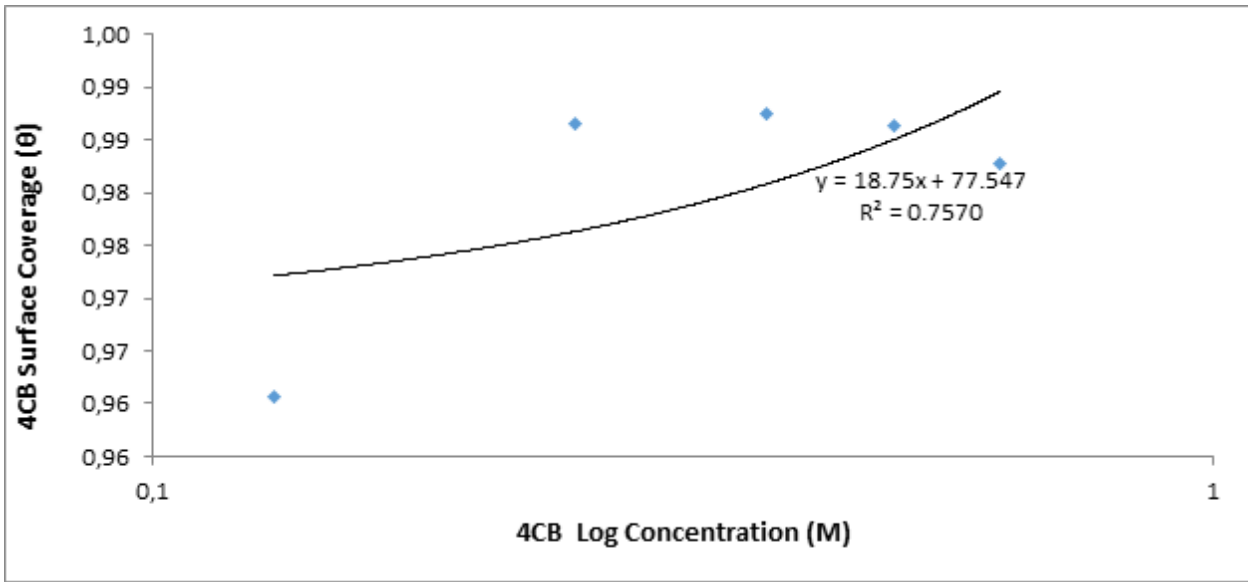

Fig. 7. Freundlich isotherm plot of 4CB for 4CB adsorption on 2101SS.

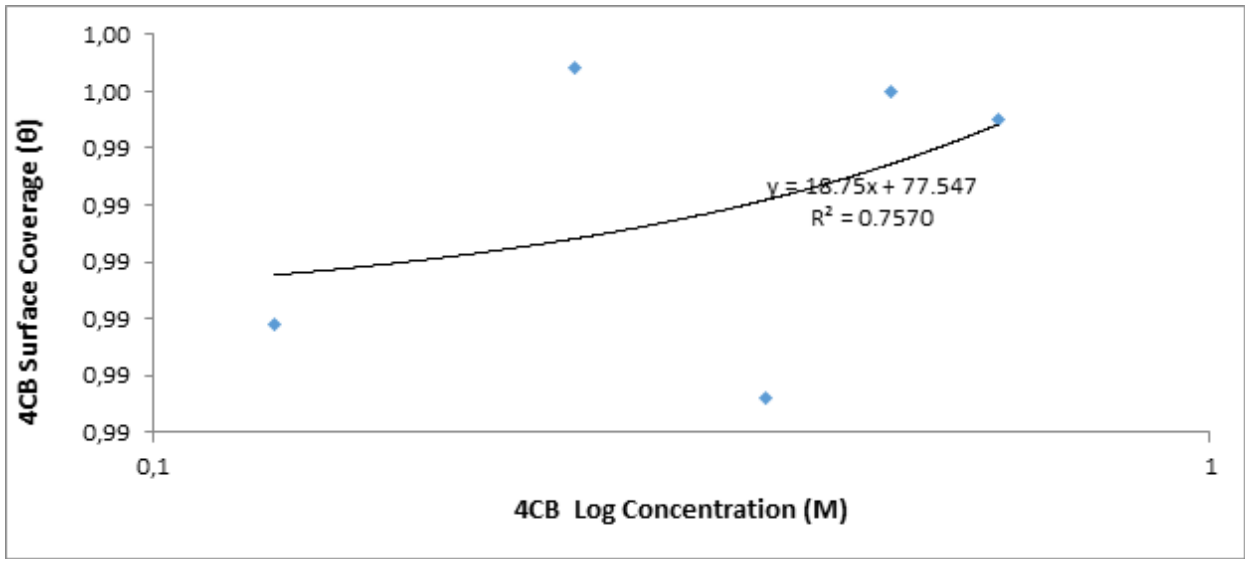

Fig. 8. Freundlich isotherm plot of 4CB for 4CB adsorption on 301SS.

where n is a constant depending on the characteristics of the adsorbed inhibitor cation, K_{ads} is the adsorption-desorption equilibrium constant representing the strength of molecular interaction within the adsorbed layer. Freundlich isotherm depicts the relationship between adsorbed 4CB cations, and their influence on the adsorption process through lateral repulsion or attraction. The amount adsorbed represents the sum total of adsorption on the reactive sites [31, 32]. The correlation coefficient for Freundlich isotherm plot (Figs. 7 and 8) is 0.7570.

Thermodynamics of the corrosion inhibition mechanism

The adsorption strength of 4CB on 2101 and 301SS was calculated from the thermodynamics of the inhibition mechanism through the equilibrium constant of adsorption from the Langmuir Isotherm due to its correlation coefficient approaching unity. Calculated results of Gibbs free energy (ΔG^{o}_{ads}) for the adsorption process is shown in Tables 6 and 7, and evaluated from the mathematical relationship below [33].

$$\Delta G_{ads} = -2.303RT \log [55.5K_{ads}] \quad (5)$$

where 55.5 is the molar concentration of water in the solution, R is the universal gas constant, T is the absolute temperature and K_{ads} is the equilibrium constant of adsorption. K_{ads} is related to surface coverage (θ) from the Langmuir equation.

Negative values of ΔG^{o}_{ads} show the adsorption reaction mechanisms is spontaneity and stable with the lowest of ΔG^{o}_{ads} value of -25.21 KJ mol^{-1} at 2.5 % 4CB and the highest ΔG^{o}_{ads} value of -28.11 KJ mol^{-1} at 1 % 4CB on 2101SS surface. On 301SS surface, the highest ΔG^{o}_{ads} value is -30.80 KJ mol^{-1} at 1 % 4CB and the lowest value of -27.74 KJ mol^{-1} at 1.5 % 4CB. The ΔG^{o}_{ads} values for both steel shows physicochemical reaction i.e. partial chemical and physical interaction of 4CB molecules on the steel's surfaces [34 - 35]. The values are generally higher for 310SS compared to 2101SS, probably due to the higher corrosion rate of 301SS because more 4CB molecules are needed to counteract the debilitating effect of the corrosive anions on 310SS surface due to its lower chromium content and different metallurgical structure. Observing the ΔG^{o}_{ads} value for 2101SS it can be deduced that the presence of higher chromium content and duplex nature was partially sufficient to resist the effect of corrosive anions, as a result competitive absorption of 4CB molecules with oxygen necessary for the formation of the passive film occurred resulting in the displacement of some 4CB molecules which might be responsible for the weak molecular interaction of 4CB on 2101SS surface, hence the lower ΔG^{o}_{ads} values. As the concentration of 4CB increased, more, excess molecules are displaced resulting in physisorption adsorption mechanism at 2.5 % 4CB. The decrease in ΔG^{o}_{ads} value was also observed for 301SS confirming the description earlier stated.

Optical microscopy analysis

Optical microscopic images of 2101SS and 301SS morphology before corrosion, after corrosion without 4CB and in the presence of 4CB after corrosion are shown on Fig. 9(a) to Fig. 11(b) at mag. x100. The morphology of the stainless steels before corrosion, Fig.

Table 6. Data for Gibbs free energy (ΔG^{o}_{ads}), surface coverage (θ) and equilibrium constant of adsorption (K_{ads}) for 4CB adsorption on 2101.

Specimen	4CB Concentration (M)	Surface Coverage (θ)	Equilibrium Constant of adsorption (K_{ads})	Gibbs Free Energy, ΔG ($Kjmol^{-1}$)
1	0	0	0	0
2	2.42E-02	0.961	1008.6	-27.09
3	4.85E-02	0.987	1518.4	-28.11
4	7.27E-02	0.988	1086.7	-27.28
5	9.70E-02	0.986	743.0	-26.33
6	1.21E-01	0.983	472.7	-25.21

Table 7. Data for Gibbs free energy (ΔG^{o}_{ads}), surface coverage (θ) and equilibrium constant of adsorption (K_{ads}) for 4CB adsorption on 301SS.

Specimen	4CB Concentration (M)	Surface Coverage (θ)	Equilibrium Constant of adsorption (K_{ads})	Gibbs Free Energy, ΔG ($Kjmol^{-1}$)
1	0	0	0	0
2	2.42E-02	0.991	4499.6	-30.80
3	4.85E-02	0.995	4461.7	-30.78
4	7.27E-02	0.990	1308.9	-27.74
5	9.70E-02	0.995	2051.5	-28.85
6	1.21E-01	0.995	1494.4	-28.07

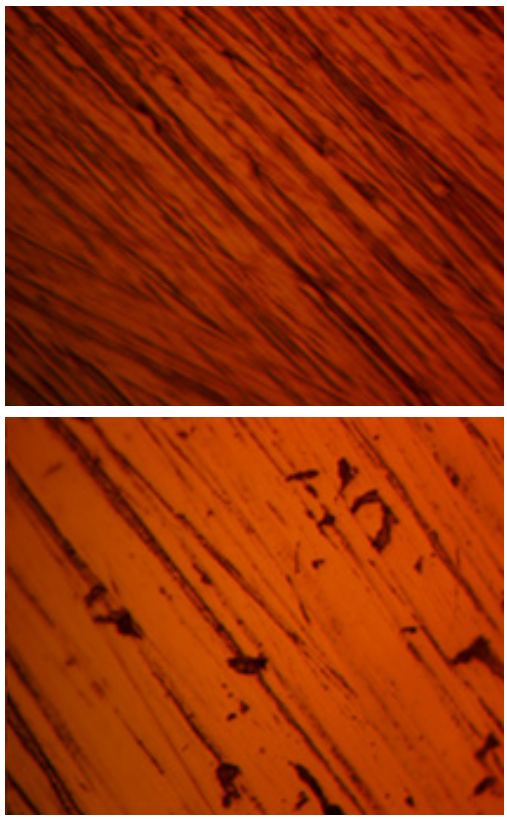

Fig. 9. Optical images of stainless steel specimen before corrosion test (a) 2101SS at mag. x100, (b) 301SS at mag. x100.

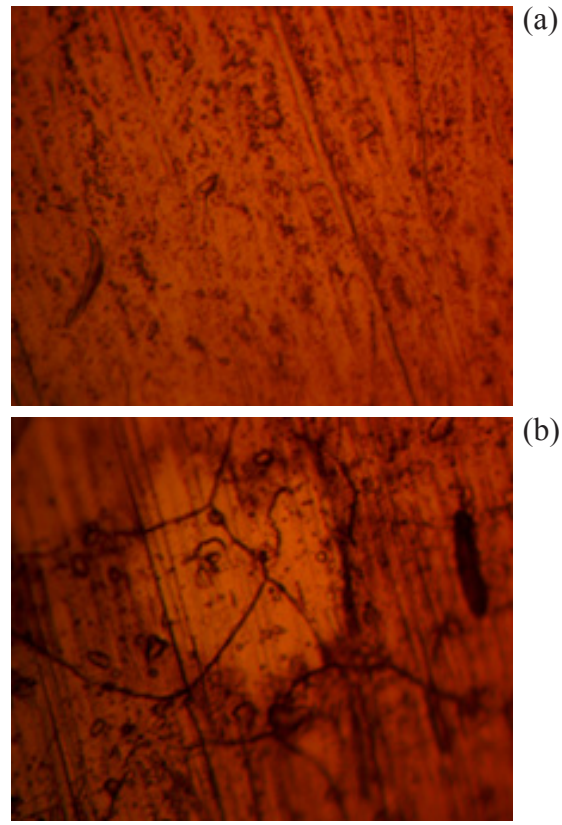

Fig. 10. Optical images of stainless steel specimen after corrosion test without 4CB (a) 2101SS at mag. x100, (b) 301SS at mag. x100.

9(a) - 9(b), depicts a mildly polished surface with serrated edges due to machining. The lined surface is more evident on 2101SS compared to 301SS despite undergoing the same metallographic treatment. Surface flaws or inclusions are visible on 30SS due to differences in its metallurgical structure. In the presence of high molar concentrations SO_4^{2-} ions (6M) without 4CB inhibitor, both steels, Fig. 10(a) and (b), undergo surface oxidation associated with corrosion. Comparing Fig. 10(a) and 10(b) with Fig. 9(a) and 9(b), the serrated edges on both steels has disappeared due to corrosion, however the corrosive effect of SO_4^{2-} ions is much more visible on 301SS, Fig. 10(b). 2101SS, Fig. 10(a), simply wear out due to its relatively higher oxidation resistance from corrosion rate results, but 301SS corroded to the point where the grain boundary of the steel is visible due to intergranular corrosion. Corrosion pits probably due to dissolution of inclusion or impurities are also presence in contrast to 2101SS which appears to be relatively smooth. In the presence of 4CB inhibitor the serrated edges are visible on 2101SS morphology, Fig. 11(a), due to the excellent inhibition property of 4CB coupled with the inherent corrosion resistance of the steel as previously discussed under adsorption isotherm where the ΔG^o_{ads} was much lesser than values obtained for 301SS due to competitive adsorption on 2101SS surface. The change in surface morphology for 2101SS is quite minimal, however studying the surface morphology of 301SS before and after corrosion in the presence of 4CB, the different is quite visible. Though the inhibited 301SS surface tends to be much smoother due to the controlled diffusion of SO_4^{2-} ions whose effects are debilitating on the steel, the initiation of macro pits are visible on the inhibited steel coupled with the presence of the grain boundary resulting from intergranular corrosion. This observation has been explained under the potentiodynamic section whereby 301SS with its lower corrosion resistance, excess SO_4^{2-} ions preadsorbs on the steel before their electrochemical action are stifled by cationic 4CB molecules.

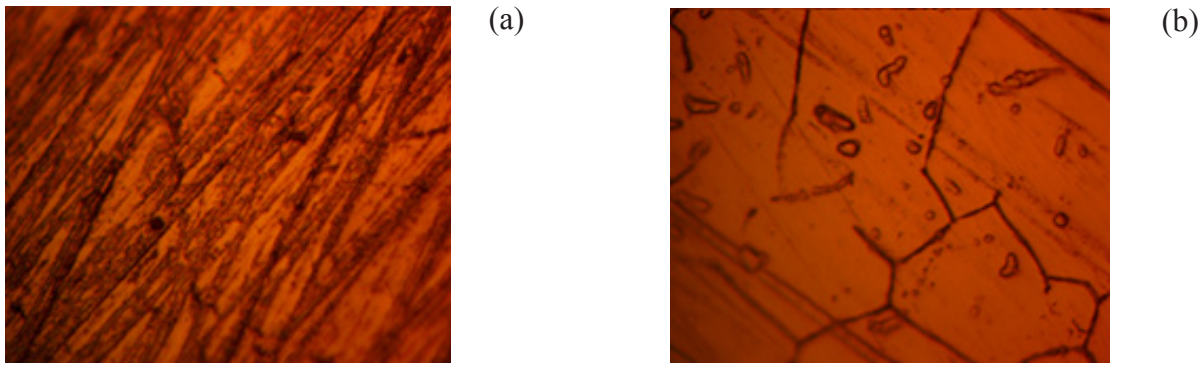

Fig. 11. Optical image of stainless steel specimen after corrosion test with 4CB (a) 2101SS at mag. x100, (b) 301SS at mag. x100.

CONCLUSIONS

4CB effectively inhibited the corrosion and surface oxidation of 2101SS and 301SS steel in dilute H_2SO_4 acid solution, but performed more effective on 2101SS from electrochemical analysis and corrosion potential monitoring. The compound selectively adsorbed onto both steels through physiochemical mechanism according to the Langmuir and Freundlich adsorption isotherm. Identified functional groups of 4CB molecular structure partially adsorbed onto both steels from analysis of the adsorption spectra. Pre-adsorption of the steel by corrosive anions and protonation of the inhibitor functional group caused a strong electrostatic attraction leading to a well passivated steel surface. The optical images of the inhibited steel specimens significantly contrast the images without 4CB compound due to formation of a protective film on the inhibited steel which hindered the diffusion of corrosive anions onto the metal-inhibitor interface.

Acknowledgements

The author acknowledges Covenant University Ota, Ogun State, Nigeria, for the sponsorship and provision of research facilities for this project.

REFERENCES

1. X. Li, T. Bell, Corrosion properties of plasma nitrided AISI 410 martensitic stainless steel in 3.5 % NaCl and 1 % HCl aqueous solutions, Corros. Sci., 48, 8, 2006, 2036-2049.
2. M.D. Pereda, C.A. Gervasi, C.L. Llorente, P.D. Bilmes, Microelectrochemical corrosion study of super martensitic welds in chloride-containing media, Corros. Sci., 53, 12, 2011, 3934-3941.
3. G. Schmitt, K. Bedbur, in: Proceedings of the Ninth International Congress on Metallic Corrosion, Toronto, Canada, 1984, 122.
4. X. Li, S. Deng, G. Mu, Q. Qu, The synergistic inhibition effect of rare earth cerium (IV) ion and iso-vanillin on the corrosion of cold rolled steel in 1.0 M H_2SO_4 solution, Mats. Letts., 61, 11-12, 2007, 2514-2517.
5. E.E. Oguzie, Y. Li, F.H. Wang, Effect of surface nanocrystallization on corrosion and corrosion inhibition of low carbon steel: Synergistic effect of methionine and iodide ion, Electrochim. Acta., 52, 24, 2007, 6988-6996.
6. E.E. Oguzie, Y. Li, F.H. Wang, Corrosion inhibition and adsorption behavior of methionine on mild steel in sulphuric acid and synergistic effect of iodine ion, J. of Colloid and Inter Sci., 310, 1, 2007, 90-98.
7. Z. Szklarska-Smialowska, Pitting Corrosion of Metals, TX. NACE, Houston, 1986.
8. B. Mernari, H. El Attari, M. Traisnel, F. Bentiss, M. Lagrenee, Inhibiting effects of 3,5-bis(n-pyridyl)-4-amino-1,2,4-triazoles on the corrosion for mild steel in 1 M HCl medium, Corros. Sci., 40, 2-3, 1998, 391-399.
9. I. Singh, Inhibition of steel corrosion by thiourea derivatives, Corrosion, 49, 3, 1993, 473-478.
10. B.G. Ateya, B.E. El-Anadouli, F.-M. El-Nizamy, The adsorption of thiourea on mild steel, Corros. Sci., 24, 6, 1984, 509-515.
11. ASTM G1 - 03(2011), Standard Practice for Preparing, Cleaning, and Evaluating Corrosion Test Specimens. http://www.astm.org/Standards/G1 (accessed 30:05:16).

12. ASTM G59 - 97(2014). Standard Test Method for Conducting Potentiodynamic Polarization Resistance Measurements. http://www.astm.org/Standards/G31 (accessed 30:05:16).
13. ASTM G102-89(2015)e1. Standard Practice for Calculation of Corrosion Rates and Related Information from Electrochemical Measurements, http://www.astm.org/Standards/G31 (accessed 30:05:16).
14. Basics of corrosion measurements. http://www.che.sc.edu/faculty/popov/drbnp/ECHE789b
15. /Corrosion%20Measurements.pdf (accessed 06:04:17).
16. ASTM G69–12. Standard test method for measurement of corrosion potentials of aluminum alloys. https://www.astm.org/Standards/G69.htm (accessed 30:05:2016).
17. P.T. Jakobsen, E. Maahn, Temperature and potential dependence of crevice corrosion of AISI 316 stainless steel, Corros. Sci., 43, 9, 2001, 1693-1709.
18. W.B. Jensen, The Lewis acid-base concepts, John Wiley & Sons, Inc., New York. 1980, 112-336.
19. J.O. Bockris, D. Drazic, A.R. Despic, The electrode kinetics of the deposition and dissolution of iron, Electrochim. Acta, 4, 2-4, 1961, 325-361.
20. J.O. Bockris, H. Kita, Analysis of galvanostatic transients and application to the iron electrode reaction, J. of the Elect. Soc., 108, 7, 1961, 676-685.
21. R.T. Loto, C.A. Loto, A.P.I. Popoola, Inhibition effect of deanol on mild steel corrosion in dilute sulphuric acid, South African J. of Chem., 68, 2015, 105-114.
22. A. Fattah-Alhosseini, A. Saatchi, M.A. Golozar, K. Raeissi, The transpassive dissolution mechanism of 316L stainless steel, Electrochim. Acta, 54, 13, 2009, 3645-3650.
23. C. Courty, H.J. Mathieu, D. Landolt, Surface oxidation of an electrochemically polarized FeCr alloy studied by SIMS oxygen isotope ratio profiling, Electrochim. Acta, 36, 10, 1991, 1623-1630.
24. J. Kruger, Uhlig's Corrosion Handbook, in: Winstone, R.R. (Ed.), John Wiley& Sons Inc. 2001.
25. M. Bojinov, G. Fabricius, T. Laitinen, T. Saario, Transpassivity mechanism of iron–chromium–molybdenum alloys studied by AC impedance, DC resistance and RRDE measurements, Electrochim. Acta, 44, 24, 1999, 4331-4343.
26. G.C. Wood, J.A. Richardson, M.F. Abd Rabbo, L.B. Mapa, W.H. Sutton, The role of flaws in breakdown of passivity of aluminum and crevice corrosion of stainless steel, R.P. Frankenthal, J. Kruger, Passivity of Metals, The Electrochemical Society, Princeton, NJ. 1978, 973-988.
27. Table of Characteristic IR Absorptions, http://orgchem.colorado.edu/Spectroscopy/specttutor/irchart.pdf. (accessed 12/01/2017).
28. S. George, Infrared and Raman Characteristic Group Frequencies: Tables and Charts. John Wiley & Sons, New York, 2004.
29. J. Zhu, Th. Hartung, D. Tegtmeyer, H. Baltruschat, J. Heitbaum, The electrochemical reactivity of toluene at porous Pt electrodes, J. of Elect. Chem., 24, 1-2, 1988, 273-286.
30. K. Shimazu, H. Kita, Hydrogenation of 1,3-butadiene on Pd in sulfuric acid solution: II. Adsorbed hydrogen species, J. of Catal., 83, 2, 1983, 407-414.
31. R. Guidelli, Adsorption of molecules at metal electrodes, Kowski, J.L. & Ross, P.N (eds.), VCH Publishers, lnc., Ncw York, 1992, p. 1.
32. S. Arivoli, K. Kalpana, R. Sudha, T. Rajachandrasekar, Comparative study on the adsorption kinetics and thermodynamics of metal ions onto acid activated low cost pandanus carbon, E-J. of Chem., 4, 2, 2007, 238-254.
33. K.S. Ashish, M.A. Quraishi, Investigation of the effect of disulfiram on corrosion of mild steel in hydrochloric acid solution, Corros. Sci., 53, 4, 2011, 1288-1297.
34. C.Aharoni, M. Ungarish, Kinetics of activated chemisorption. Part 2. Theoretical models, J. of the Chem. Soc. Faraday Trans., 73, 1977, 456-464.
35. R.T. Loto, C.A. Loto, T. Fedotova, Inhibition effect of n, n'-dimethylaminoethanol on the corrosion of austenitic stainless steel type 304 in 3M H_2SO_4, Int. J. Elect. Sci., 7, 2012, 10763-10778.
36. R.T. Loto, C.A. Loto, A.P.I. Popoola, T.T. Fedotova, Inhibition effect of 2-amino, 5-ethyl- 1, 3, 4 thiadiazole on the corrosion of austenitic stainless steel type 304 in dilute sulphuric acid, Port. Electrochim. Acta, 32, 5, 2014, 337-354.